# Dynamic Harmonic Synchrophasor Estimator based on Sinc Interpolation Functions

Lei Chen, Wei Zhao, Qing Wang, *Senior Member, IEEE*, Fuping Wang, and Songling Huang, *Senior Member, IEEE*.

***Abstract*—This paper introduces a new dynamic harmonic synchrophasor estimator (DHSE) based on the Shannon sampling theorem. Each dynamic harmonic phasor is modeled as a weighted sum of a series of sinc interpolation functions. Based on this, a bank of finite impulse response filters is designed. They are used to estimate not only the dynamic harmonic synchrophasor but also the harmonic frequency and rate of change of frequency (ROCOF). A model parameter is properly selected to obtain good performance, both in low- and high-order harmonics estimation. Frequency responses and simulation tests are used to compare the performances of the DHSE and the Taylor-Fourier transform (TFT). Results show that the DHSE has lower passband ripples and higher stopband attenuation than the TFT. Moreover, under frequency deviation, harmonic oscillation and frequency ramp conditions, the DHSE is more accurate than the TFT in dynamic harmonic synchrophasor, frequency and ROCOF estimation.**

***Index Terms*—dynamic harmonic, finite impulse response filter, harmonic synchrophasor, harmonic frequency, rate of change of frequency (ROCOF), sinc interpolation function.**

## I. Introduction

NOWADAYS, dynamic harmonics are widely present in power system voltage/current signals. For example, adjustable speed devices can cause dynamic current harmonics during changing speeds. Also, subsynchronous resonance can result in harmonic amplitude and frequency oscillations [1]. Thus, it is essential to estimate dynamic harmonic phasors simultaneously for smart mitigation device operations and subsynchronous resonance monitoring [2]-[5].

Phasor measurement units (PMUs) are widely used in power systems to track dynamic behaviors of power systems in synchronisation. In the future, PMUs are also expected to play an important role in dynamic harmonic synchrophasor measurement. In [6] and [7], a harmonic PMU prototype was designed for harmonic synchrophasor estimation. However, as far as we know, there is no standard for harmonic synchrophasor measurement. No test conditions and metrics can be followed to test a harmonic synchrophasor estimator. The IEEE Synchrophasor Standard [8], [9] (called the Standard in the following) is only in correspondence with the fundamental synchrophasor measurement. It states that quantities including fundamental synchrophasor, frequency and rate of change of frequency (ROCOF) should be estimated with a required accuracy, even under dynamic conditions. Accordingly, the goal of this paper is to develop a dynamic harmonic synchrophasor, frequency and ROCOF estimator with a high accuracy and limited computational complexity.

Traditionally, the discrete Fourier transform (DFT) (or the fast Fourier transform) was widely used for harmonic synchrophasor estimation due to its simplicity and low computational cost [6], [7], [10]. However, it is not suitable for dynamic harmonic synchrophasor estimation. This is because it assumes the analyzed signal is periodic. As a result, spectral leakage and mutual harmonic interference will be present. Window functions and harmonic group-based methods were applied in [1] and [11] to mitigate these impacts.

Recently, a dynamic harmonic phasor model was well established in the Taylor-Fourier transform (TFT) [5] and the Taylor-Kalman-Fourier (TKF) filters [12]. The TFT and TKF can return harmonic phasor derivatives. Thus, not only the dynamic harmonic synchrophasor can be estimated but also harmonic frequency and ROCOF. Additionally, they are much more accurate than the classical DFT because of the well-designed maximally flat filters. Inspired by the TFT, many Taylor signal model-based methods, such as the Taylor-Kalman filter [13], [14], were also proposed for dynamic harmonic synchrophasor estimation. However, these Taylor signal model-based methods share a problem of large errors under frequency deviation conditions [15], especially when high-order harmonics are considered. In order to widen the frequency range of the TFT, adaptive TFTs with the use of lookup tables, phase-locked loop filters or frequency-locked loop filters were proposed in [16]-[18]. However, larger memory storage and/or higher computational burden are the price to pay to outperform the classical TFT.

Regarding interharmonic interferences, the Taylor-Fourier multifrequency model-based methods [19]-[22] are useful tools for this problem. However, they have to sacrifice computation time on measurement matrix generation. Other methods, such as the Kalman filter bank [1], [10], the multiple resonator [2], and the estimation of signal parameters using a rotational invariance technique [23], were also proposed for dynamic harmonic synchrophasor estimation in various areas.

As for dynamic harmonic synchrophasor estimation, the challenge is that high-order harmonics have wider frequency bands than low-order harmonics. As discussed above, the widely used TFT has large errors in high-order harmonics estimation. This paper expects to cope with this problem by developing a new phasor model to describe dynamic harmonics.

Lei Chen, Wei Zhao, Fuping Wang, and Songling Huang are with the State Key Lab. of Power System, Department of Electrical Engineering, Tsinghua University, Beijing, 100084, China. Qing Wang is with the School of Engineering and Computer Sciences, Durham University, Durham, UK (e-mail: chenleithu@hotmail.com; zhaowei@mail.tsinghua.edu.cn).

We demand that the corresponding estimator's passband performances could be flexibly modified by a model parameter. In this way, good performance can also be obtained for high-order harmonics.

To this end, a new model is developed based on the Shannon sampling theorem, where the sampling frequency can be flexibly modified to modify passband and/or stopband performance. This model helps us to design a bank of finite impulse response (FIR) filters for dynamic harmonic synchrophasor, frequency, and ROCOF estimation.

Although the passband can be widened by adopting a window function (e.g., the Kaiser window) or a first frequency estimation [16-18], this paper would like to deal with this problem from the perspective of the model. Moreover, a window function can be used to widen the passband of the proposed method again. In the following, the proposed dynamic harmonic synchrophasor estimator is called the DHSE.

This paper is organized as follows. First, the principles of the DHSE are introduced in section II. Next, the parameters impacting on the frequency responses of the DHSE are analyzed in section III. Then, practical implementation items of the DHSE are discussed in section IV. Afterwards, the DHSE and TFT are tested and compared under steady state and dynamic conditions. Also, a practical example is taken to show the practical value of the DHSE. Finally, the main conclusions of the DHSE are given.

## II. Dynamic Harmonic Synchrophasor Estimator

### A. Signal Model Foundation

In the Standard, a fundamental synchrophasor is defined as a fundamental phasor referring to the nominal frequency $f_0$. In this paper, the concept of the fundamental synchrophasor is extended to harmonic components. Thus, the $h$th harmonic synchrophasor refers to the harmonic frequency $hf_0$. In this way, a signal with dynamic harmonics can be defined as

$$\begin{aligned} s(t) &= \sqrt{2}\sum_{h=1}^{H} a_h(t)\cos\left(2\pi h f_0 t + \theta_h(t)\right) \\ &= \sqrt{2}\,\mathrm{Re}\left\{\sum_{h=1}^{H} p_h(t) e^{j2\pi h f_0 t}\right\} \end{aligned} \tag{1}$$

where $\mathrm{Re}\{\cdot\}$ denotes the operator returning the real part of the phasor; $H$ is the maximum harmonic order; $f_0$ is the nominal fundamental frequency; and $p_h(t)= a_h(t)e^{j\theta_h(t)}$ is the $h$th harmonic synchrophasor, in which $a_h(t)$ and $\theta_h(t)$ are the magnitude (RMS value) and phase oscillations of the $h$th harmonic.

Generally, a dynamic harmonic synchrophasor $p_h(t)$ can be assumed band-limited [24]. According to [25] and [26], each band-limited signal $p_h(t)$ can be approximately modelled as a weighted sum of a series of sinc interpolation functions (more derivations can be found in Appendix), which is given by

$$\begin{aligned} p_h^K(t) = \sum_{k=-K}^{+K} p_{k,h}\frac{\sin\left[\pi\left(2B_h t-k\right)\right]}{\pi\left(2B_h t-k\right)} \qquad & h=1,\ldots,H \\ -\frac{T_\mathrm{w}}{2}\le t\le\frac{T_\mathrm{w}}{2} & \end{aligned} \tag{2}$$

where $B_h$ is a frequency greater than the maximum frequency of the baseband signal $p_h(t)$ ($B_h\neq 0$); $p_{k,h}=p_h(k/(2B_h))$ is the sample of $p_h(t)$ at $t=k/(2B_h)$ with the sampling rate $2B_h$; and $K$ is the sample number on both sides of $p_h(0)$. Thus, $2K$ can be seen as the model order. Moreover, the observation window $T_\mathrm{w}$ should meet $T_\mathrm{w}<K/B_h$.

### B. Filter Bank Design

Assume the signal is sampled at $N_0$ samples per cycle $T_0=1/f_0$. $N_w=N_0(T_\mathrm{w}/T_0)$ is the sample number corresponding to the observation interval $T_\mathrm{w}$. Note that $N_\mathrm{w}$ should be an odd number to make $t_0=0$ at the center of the observation window. In this way, there are $N$ samples at both sides of $t_0=0$, and thus $N_\mathrm{w}=2N+1$. $c=[N_\mathrm{w}/N_0]$ is the integer cycle number of the observation window, where [ ] is the operation picking the closest integer. Then, (1) can be rearranged as

$$\mathbf{s} = \frac{\sqrt{2}}{2}\begin{bmatrix}\boldsymbol{\Phi}_R & \boldsymbol{\Phi}_I\end{bmatrix}\begin{bmatrix}\mathbf{c}_K \\ \mathbf{c}_K^*\end{bmatrix} = \frac{\sqrt{2}}{2}\boldsymbol{\Phi}\mathbf{p}, \tag{3}$$

where $\mathbf{s}\in R^{N_\mathrm{w}}$ is a column vector consisting of $N_w$ samples of the signal $s(t)$; $\boldsymbol{\Phi}_R\in C^{N_\mathrm{w}\times H(2K+1)}$ and $\boldsymbol{\Phi}_I\in C^{N_\mathrm{w}\times H(2K+1)}$ are two matrices consisting of $N_w$ samples of the basis functions $\phi_{k,h}^R(n)$ (see (4)) and $\phi_{k,h}^I(n)$ (see (5)) in each column; $\mathbf{p}_K\in C^{H(2K+1)}$ and $\mathbf{p}_K^*\in C^{H(2K+1)}$ are two column vectors consisting of the harmonic synchrophasor samples (see (6) and (7)).

$$\begin{aligned} \phi_{k,h}^R(n) = \frac{\sin\left[\pi\left(2B_h nT_\mathrm{s}-k\right)\right]}{\pi\left(2B_h nT_\mathrm{s}-k\right)} e^{j2\pi h f_0 nT_\mathrm{s}} \\ k=-K,\ldots,K \\ h=1,\ldots,H \end{aligned} \tag{4}$$

$$\begin{aligned} \phi_{k,h}^I(n) = \frac{\sin\left[\pi\left(2B_h nT_\mathrm{s}-k\right)\right]}{\pi\left(2B_h nT_\mathrm{s}-k\right)} e^{-j2\pi h f_0 nT_\mathrm{s}} \\ k=-K,\ldots,K \\ h=1,\ldots,H \end{aligned} \tag{5}$$

$$\mathbf{p}_\mathrm{K} = \left[p_{-\mathrm{K},1},\ldots,p_{\mathrm{K},1},\ldots,p_{-\mathrm{K},h},\ldots,p_{\mathrm{K},h},\ldots,p_{-\mathrm{K},\mathrm{H}},\ldots,p_{\mathrm{K},\mathrm{H}}\right]^T \tag{6}$$

$$\mathbf{p}_\mathrm{K}^* = \left[p_{-\mathrm{K},1}^*,\ldots,p_{\mathrm{K},1}^*,\ldots,p_{-\mathrm{K},h}^*,\ldots,p_{\mathrm{K},h}^*,\ldots,p_{-\mathrm{K},\mathrm{H}}^*,\ldots,p_{\mathrm{K},\mathrm{H}}^*\right]^T \tag{7}$$

Then the least squares method can be used to realize the optimal estimation of $\mathbf{p}$, which is given by

$$\hat{\mathbf{p}}=\sqrt{2}\left(\boldsymbol{\Phi}^H\boldsymbol{\Phi}\right)^{-1}\boldsymbol{\Phi}^H\mathbf{s} \tag{8}$$

where $^H$ is the Hermitian operator. In (8), the matrix $\boldsymbol{\Phi}^+=(\boldsymbol{\Phi}^H\boldsymbol{\Phi})^{-1}\boldsymbol{\Phi}^H=(\Phi_{i,j})\in C^{[2H(2K+1)]\times N_\mathrm{w}}$ contains the impulse responses of the FIR filters for harmonic synchrophasor samples estimation. Let

$$\begin{aligned} \mathbf{g}_{k,h} = [&\Phi_{(h-1)\times(2K+1)+(k+K+1),0},\cdots,\Phi_{(h-1)\times(2K+1)+(k+K+1),n}, \\ &\cdots,\Phi_{(h-1)\times(2K+1)+(k+K+1),N_\mathrm{w}-1}] \qquad h=1,\ldots,H \end{aligned} \tag{9}$$

be a row vector consisting of the impulse responses of the filters, in which $\Phi_{(h\text{-}1)\times(2K+1)+(k+K+1),n}$ is the matrix elements corresponding to the basis function $\phi_{k,h}^R(n)$; $((h\text{-}1)\times(2K+1)+(k+K+1))$ is the row number of $\boldsymbol{\Phi}^+$. The FIR filters for harmonic synchrophasor samples estimation are the time-inverse version of $\mathbf{g}_{k,h}$, which is given by

$$\begin{aligned} h_{k,h}(n) = g_{k,h}(-n+N_\mathrm{w}-1) \qquad & h=1,\ldots,H \\ & n=0,\ldots,N_\mathrm{w}-1 \end{aligned} \tag{10}$$

### C. Dynamic Harmonic Synchrophasor, Frequency and ROCOF Estimation

Based on the filters designed above, harmonic synchrophasor samples can be estimated by

$$\hat{p}_{k,h}=\sqrt{2}\left[\sum_{n=0}^{N_w-1}h_{k,h}(n)s\left(t_0-(n-N)T_s\right)\right]e^{-j2\pi hf_0t_0} \quad h=1,\ldots,H \tag{11}$$

According to (3), dynamic harmonic synchrophasors and their derivatives can be estimated by the above estimated samples, which is given by

$$\begin{aligned} p_h^{K(m)}(t)\Big|_{t=t_0} &= \frac{d^m}{dt^m}\left(\sum_{k=-K}^{+K}\hat{p}_{k,h}\frac{\sin\left[\pi\left(2B_ht-k\right)\right]}{\pi\left(2B_ht-k\right)}\right)\Bigg|_{t=t_0} \\ &= \left[\sum_{k=-K}^{+K}\hat{p}_{k,h}\frac{d^m}{dt^m}\left(\frac{\sin\left[\pi\left(2B_ht-k\right)\right]}{\pi\left(2B_ht-k\right)}\right)\right]\Bigg|_{t=t_0} \end{aligned} \tag{12}$$

Typically, let $K$=1. After some deductions on (12), we can obtain

$$\begin{aligned} p_h^{1(0)}(t_0)&=\hat{p}_{0,h} \\ p_h^{1(1)}(t_0)&=2B_h\left(\hat{p}_{1,h}-\hat{p}_{-1,h}\right) \\ p_h^{1(2)}(t_0)&=4B_h^2\left(2\hat{p}_{1,h}+2\hat{p}_{-1,h}-\frac{\pi^2}{3}\hat{p}_{0,h}\right) \end{aligned} \tag{13}$$

According to the first equation in (13), $h_{0,h}(n)$ can be used as the filter for the $h$th harmonic synchrophasor $p_h^{K(0)}$ estimation (even if $K\neq1$, the first equation is still satisfied). On the basis of the derivatives of harmonic synchrophasors, harmonic frequency and ROCOF can also be estimated [24], [27], which is given by

$$\hat{f}_h=hf_0+\frac{1}{2\pi}\frac{\mathrm{Im}\left\{p_h^{K(1)}(t_0)\,p_h^{K(0)*}(t_0)\right\}}{\left|p_h^{K(0)}(t_0)\right|^2} \tag{14}$$

$$\begin{aligned} ROCOF_h=&\frac{1}{2\pi}\frac{\mathrm{Im}\left\{p_h^{K(2)}(t_0)\,p_h^{K(0)*}(t_0)\right\}}{\left|p_h^{K(0)}(t_0)\right|^2} \\ &-\frac{1}{\pi}\frac{\mathrm{Re}\left\{p_h^{K(1)}(t_0)\,p_h^{K(0)*}(t_0)\right\}\mathrm{Im}\left\{p_h^{K(1)}(t_0)\,p_h^{K(0)*}(t_0)\right\}}{\left|p_h^{K(0)}(t_0)\right|^4} \end{aligned} \tag{15}$$

where Im{ } denotes the operator returning the image part of the phasor and $^*$ denotes the conjugate operation. The latency of the harmonic synchrophasor, frequency and ROCOF estimator is

$$T_{\text{latency}}=\frac{N_w-1}{2f_s} \tag{16}$$

where $N_w-1$ is the order of the filters designed above.

## III. Flexible Selection of Parameter $B_h$ for Different Order Harmonics

Under off-nominal frequency, frequency oscillation and frequency ramp conditions, frequencies of different harmonics will have different deviations from the nominal values. For example, if the fundamental frequency has a static deviation of $\Delta f$, the $h$th harmonic will have a deviation of $\Delta f_h=h\Delta f$. In this case, measurement of high-order harmonics needs estimators with wide passbands and stopbands. However, the TFT's passbands (or stopbands) are narrow for high-order harmonics estimation.

Generally, the sinc interpolation can be seen as a low pass filter for baseband signal $p_h(t)$ filtering. The performances of the low pass filter are determined by the parameter $B_h$, and so are the DHSE's performances.[1] We can select different values of $B_h$ for different harmonics. In Fig. 1, magnitude responses of the DHSE under different values of $B_h$ are shown. As seen in Fig. 1(b) and (c), with the increase of $B_h$, the passband and stopband bandwidths also increase. Thus, we can choose a proper value of $B_1$ for fundamental phasor model foundation, and $B_h=hB_1$ is used for the $h$th harmonic. With the increase of harmonic order, the corresponding estimator's bandwidth also increases.

In the standard GB/T 15945-2008, frequency deviation in China's public power grid is limited within [-0.5, 0.5] Hz [28]. Thus, we set the fundamental frequency bandwidth to 1 Hz, and the frequency bandwidth of $h$th harmonic is accordingly $h$ Hz. In this case, $B_1$ should be bigger than the possible maximum frequency of $p_1(t)$, i.e., 0.5 Hz. For example, through a large number of simulations, we set $B_1$=0.575 Hz to get good passband and stopband performances around each harmonic frequency.

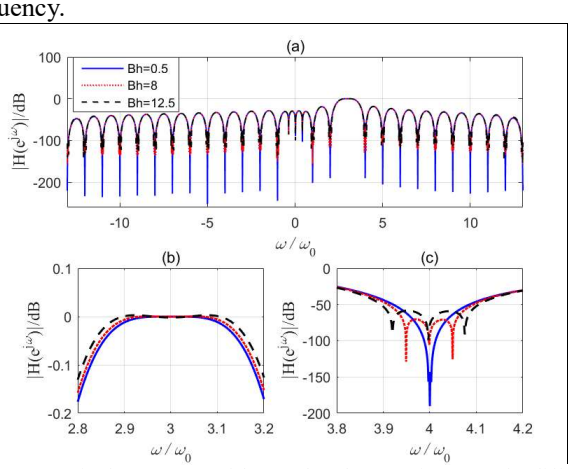


Fig. 1. Magnitude responses of the synchrophasor estimator under different values of parameter $B_h$. In each case, the same values of $B_h$ are selected for all harmonics. $N_0$=200, $f_0$=50Hz, $T_w$=3/$f_0$, $K$=1 and $H$=13 are selected for the DHSE. (b) and (c) are zooms around the third and fourth harmonic frequency, respectively. For better readability, only the frequency responses from −150 to 300 Hz are shown in (a).

## IV. Frequency Response

This section analyzes the performances of the estimator by its frequency response. Meanwhile, parameter $K$'s impact on the performances of the estimator are also discussed in this section. For brevity, the frequency response of the third harmonic estimator is chosen as an example. The filters for other harmonics have similar performance.

### A. General Discussions on the Performances of the Estimator

Figs. 2, 3 and 4 show the magnitude responses of the synchrophasor zeroth-derivative, first-derivative and second- derivative estimators, respectively. For the synchrophasor zeroth-derivative estimator, flat gains (band-pass) (see Fig. 2(b)) can be found around the third harmonic frequency, and null gains (band-stop) (see Fig. 2(c) and (d)) can be found around

[1]The performances of the DHSE are also determined by the parameter $K$. However, it can only be an integer like the TFT's model order. Thus, it cannot be flexibly selected for each harmonic.

other harmonic frequencies. As a result, harmonic synchrophasors can be well estimated due to the wide passband around the harmonic frequency and the wide stopband around other harmonic frequencies. Moreover, with the increase in harmonic order, the stopband around the harmonic frequency becomes wider (see Fig. 2(c) and (d)).

Similar conclusions can be drawn in other phasor derivative estimators. A wider stopband can be found around high-order harmonic frequencies (see Fig. 3(c), (d), Fig. 4(c), (d)). Please note that, around the third harmonic frequency, the first- and second-derivative estimators have linear and parabolic gains, respectively (see Fig. 3(b) and Fig. 4(b)). This is expected for harmonic frequency and ROCOF estimation.

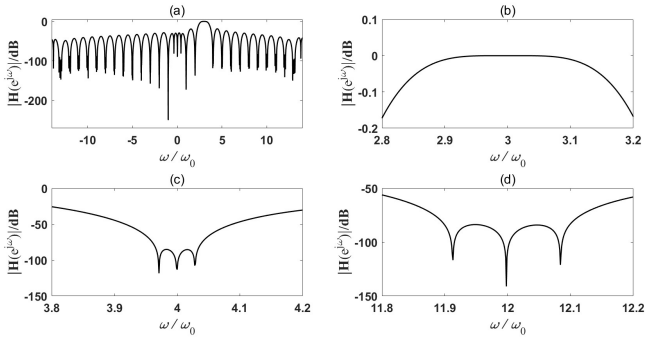


Fig. 2. Magnitude responses of the synchrophasor (zeroth-derivative) estimator. (b) for the third harmonic, (c) for the fourth harmonic and (d) for the twelfth harmonic. $N_0$=200, $f_0$=50 Hz, $T_w$=3/$f_0$, $K$=1, $B_1$=0.575 Hz, and $H$=13 are selected for the DHSE.

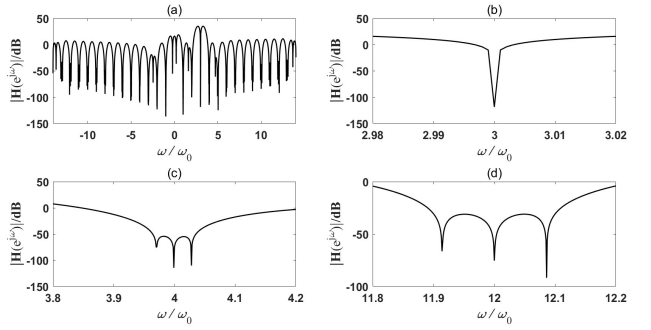


Fig. 3. Magnitude responses of the synchrophasor first-derivative estimator. (b) ((c) or (d)) is for the same harmonic shown in Fig. 2. The parameter values are selected the same as Fig. 2.

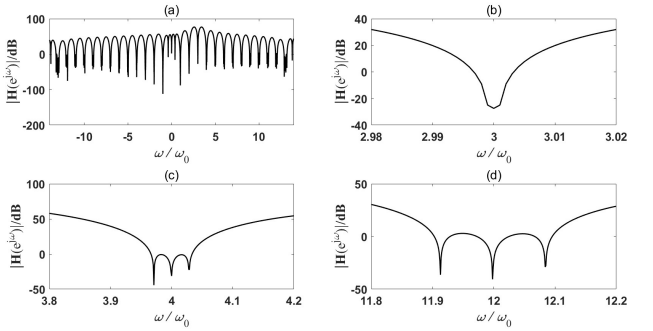


Fig. 5. Magnitude responses of the synchrophasor second-derivative estimator. (b) ((c) or (d)) is for the same harmonic shown in Fig. 2. The parameter values are selected the same as Fig. 2.

### B. *The Parameter K's Impact on the Performance of the Filters*

Generally, the parameter $K$ determines the sample numbers of the sinc interpolation-based model. Thus, it will also have impact on the filters' passband and stopband performances. In Fig. 6, the magnitude responses of the third harmonic synchrophasor estimator with different values of $K$ are shown. With the increase of $K$ (thus the signal model order also increases), the passband and stopband bandwidths increase rapidly (see Fig. 6(b) and (c)). However, the gain in transition band becomes larger, which makes the estimator sensitive to wideband noise. In practical applications, when the model order is high, a long observation window should be used to improve the filter's performance of noise suppression.

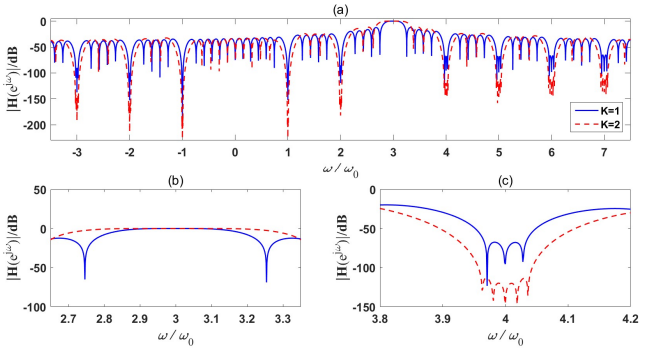


Fig. 6. Magnitude response of the synchrophasor estimator with different values of parameter $K$. $N_0$=200, $f_0$=50 Hz, $T_w$=7/$f_0$, $B_1$=0.575 Hz and $H$=13 are selected for the DHSE. For better readability, only the frequency responses from −150 to 350 Hz are shown in (a).

## V. Discussion of Practical Implementation

This section discusses the possibility of practical implementation of the DHSE. The passband ripple, stopband attenuation, filter order, latency and computational burden are discussed under different values of window length and model order. For brevity, the passband and stopband performance of the third harmonic synchrophasor estimator are taken as an example.

### A. *Practical Implementation Performances of the DHSE*

In Figs. 7, 8 and TABLE I, the DHSE's and TFT's performance with some practical values of $c$ and model order are given. Generally, when a short cycle window and low order model is used, the estimator latency is short. When a higher order model is used, a longer window should be used to get good performance, whereas the price is longer latency. Thus, the former selection of $c$ and model order is suitable for protect applications, which demand fast responses. By contrast, the latter one is suitable for precision measurement applications, which do not need fast responses.

Now we compare the performance of the DHSE and TFT. When the same length window and model order are used in the both estimators, their filter orders and latencies are the same. However, the DHSE has a smaller passband ripple and higher stopband attenuation, both around low- and high-order harmonic frequencies. For example, when they are both truncated at the second order, the DHSE's passband ripple for the third harmonic is 1.59E-5 dB, whereas the TFT's reaches 1.08E-4 dB (see Fig. 7(b)). When a longer window and higher order is used, the DHSE's passband ripple becomes lower, and its stopband attenuation become higher. It still performs better than the TFT in terms of passband and stopband performance (see Fig. 8(b), (c) and (d)).

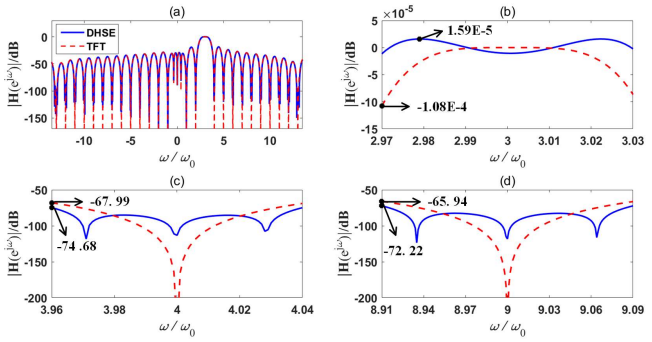


Fig. 7. Magnitude responses of the DHSE and TFT (both truncated at the second order). The fundamental passband and stopband bandwidths are both set at 1 Hz. $T_w$=3/$f_0$ is selected for the DHSE.

V

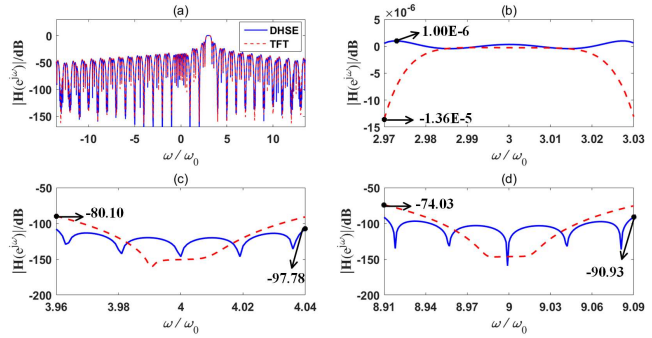


Fig. 8. Magnitude responses of the DHSE and TFT (both truncated at the fourth order). The fundamental passband and stopband bandwidths are both set at 1 Hz. $T_w$=7/$f_0$ is selected for the DHSE.

TABLE I
PERFORMANCES OF THE DHSE AND TFT. $N_0$=200 AND $f_0$=50 HZ ARE SELECTED FOR THE BOTH ESTIMATORS.

| Method | $c$ | Model order | Passband ripple /dB | Stopband attenuation /dB | | Filter order | Latency /ms |
|---|---|---|---|---|---|---|---|
| | | | | 4th | 9th | | |
| DHSE | 3 | 2 | 1.59E-5 | 74.68 | 72.22 | 598 | 29.5 |
| | 7 | 4 | 1.00E-6 | 97.78 | 90.93 | 1438 | 69.5 |
| TFT | 3 | 2 | 1.08E-4 | 67.99 | 65.94 | 598 | 29.5 |
| | 7 | 4 | 1.36E-5 | 80.10 | 74.03 | 1438 | 69.5 |

### B. Computational Burden

Generally, the filters for synchrophasor derivatives (or samples) estimation can be designed offline. Therefore, the main computations of the DHSE are for the samples estimation (the computations for harmonic frequency and ROCOF estimation are negligible) (see (11), (14), and (15)). Assume the length of an observation window is $N_w$. Then the DHSE needs $4N_w$ real multiplications and $2(N_w-1)$ real additions for a derivative estimation. The total computations for all derivatives estimation are $4*(K+1)*H*N_w$ real multiplications and $2*(K+1)*H*(N_w-1)$ real additions. Obviously, the computational burdens of the DHSE and TFT are generally the same, and are both limited. Thus, the DHSE has the possibility of practical implementation.

## VI. PERFORMANCE TESTS

In order to evaluate and compare the performances of the DHSE and TFT, several simulation tests are carried out. The total vector error (TVE), frequency error (FE) (in absolute value), and ROCOF error (RFE) (in absolute value) defined in the Standard are used to evaluate both estimators. $T_w$=3/$f_0$, $B_1$=0.575 Hz, $f_s$=10 kHz, $f_0$=50 Hz and the second order model are selected for both estimators. Please note that in China's synchrophasor measurement standard GB/T 26862-2011 [29], harmonics up to the 13th order are particularly considered. Thus, we set $H$=13 in this paper. The tests are carried out over $10^4$ runs and 250 fundamental cycles. The results within the time window [0, $T_w$/2] are not included in the statistics.

Because there are no standards for harmonic synchrophasor measurement, no test conditions and metrics can be followed. In the following tests, the IEEE Standards [8], [9] for fundamental synchrophasor measurement are mainly referred. Because the accuracy requirements for M class PMUs are stricter than P class PMUs, they are mainly referred to for accuracy evaluation. Accordingly, because the response time requirements for P class PMUs are stricter than M class PMUs, they are mainly referred for response time evaluation. The relative difference is defined as

$$r = \frac{pee_{\mathrm{TFT}} - pee_{\mathrm{DHSE}}}{pee_{\mathrm{TFT}}} \times 100\%, \qquad (17)$$

which is used to evaluate the difference between the DHSE's and TFT's parameter estimation error (PEE), i.e., TVE, FE and RFE.

### A. Frequency Deviation and Noise

This test is to evaluate the estimators' performances under frequency deviation conditions. In each test, the harmonic with order from the second to the 13th is included in the signal, respectively (see (18)). Each harmonic level is set to 10% of the fundamental, which is stated in the M class tests of the Standard. The fundamental frequency $f$ is varied from 49.5 to 50.5 Hz randomly.

$$s(t) = \cos(2\pi ft) + 0.1\cos(2\pi hft) \qquad h = 2,\ldots,13. \qquad (18)$$

In Fig. 9, the maximum TVEs, FEs and RFEs obtained with the DHSE and TFT, as well as their relative differences, are shown. We can see that the DHSE is generally more accurate than the TFT in harmonic synchrophasor, frequency and ROCOF estimation. The TFT has large errors in high-order harmonics estimation. By contrast, the DHSE's accuracy in high-order harmonics estimation are improved by at least 40%. This is because the DHSE has lower passband ripples and higher stopband attenuation for this kind of harmonics. Similar results are obtained in sections IV and V.

In the Standard, the TVE and FE limits for M class PMUs under this condition are 1% and 0.025 Hz, respectively (there is no RFE limit in the Amendment Standard [9]). If the same limits are required for harmonic components, the DHSE can only meet the TVE requirement. However, the impact of frequency deviations can be mitigated by using a longer observation window and higher order model (see TABLE I).

In another test, wideband Gaussian noise at a signal-noise-ratio of 60 dB is added in (18) ($f$=50 Hz). As is known, this noise level is common in power systems. The results are shown in Fig. 10. Although the DHSE's PEEs of high-order harmonics are larger than the TFT's, their differences in low-order harmonics are almost null. Moreover, in this condition, the TVE and FE limits can both be met.

### B. Mutual Harmonic Interferences

Harmonic parameter estimation can be interfered by other harmonics. In this test, 10% harmonics from the second to the

13th are added to a pure sine signal. The fundamental frequency is varied from 49.5 to 50.5 Hz.

The corresponding results are shown in Fig. 11. The DHSE is much more accurate than the TFT in all parameter estimation. Compared with the TFT, the DHSE's accuracies in high-order harmonics are improved by at least 40%. If the same limits given above are referred in this test, the TVE can only meet the TVE limit.

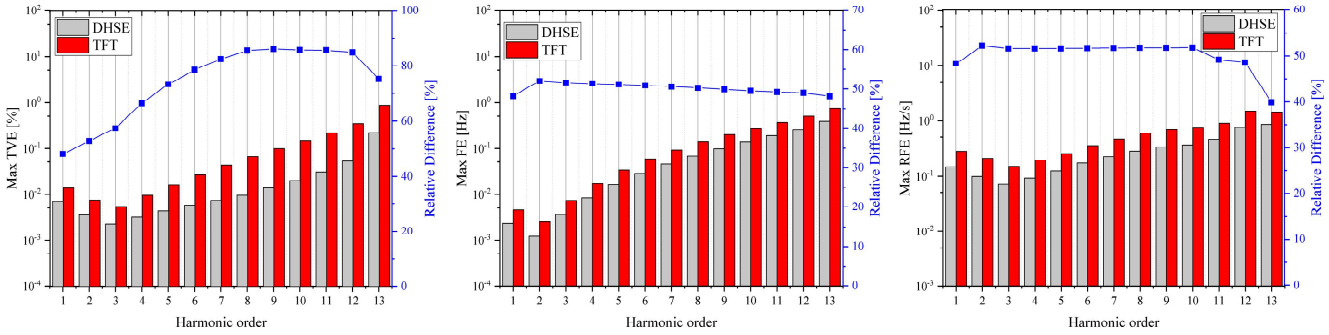


Fig. 9. Results under frequency deviation conditions ($f$=-49.5~50.5 Hz).

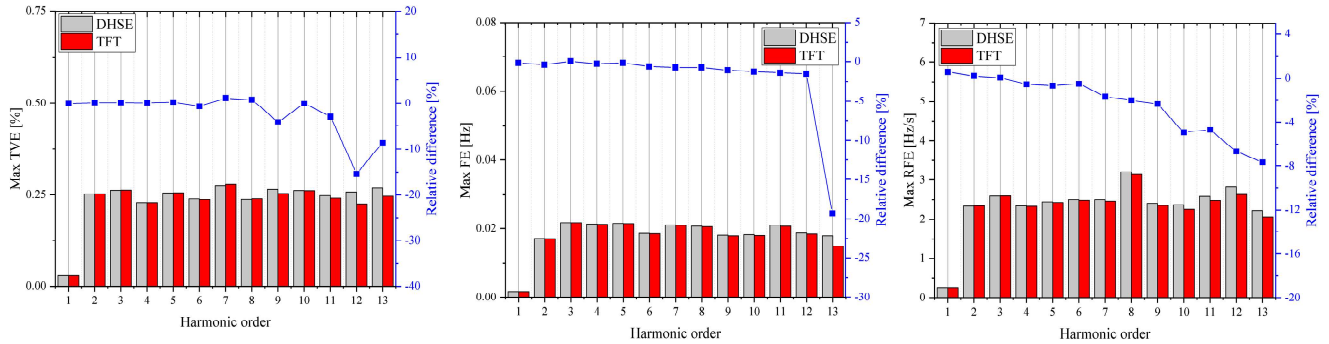


Fig. 10. Results under noise conditions (SNR=60 dB).

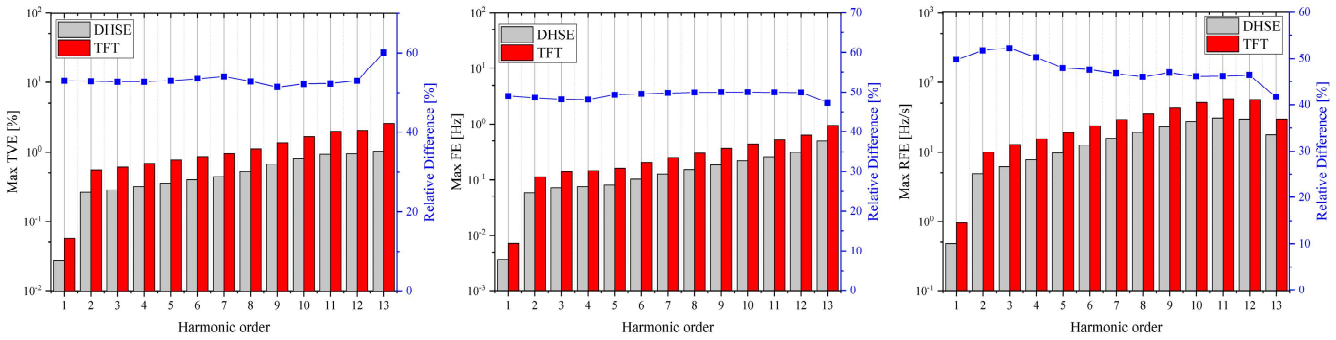


Fig. 11. Results under mutual harmonic interference conditions.

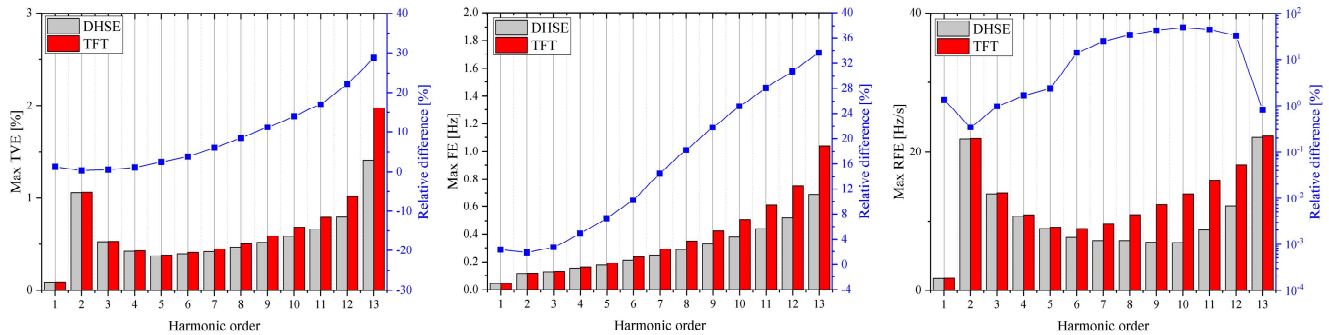


Fig. 12. Results under harmonic oscillation conditions.

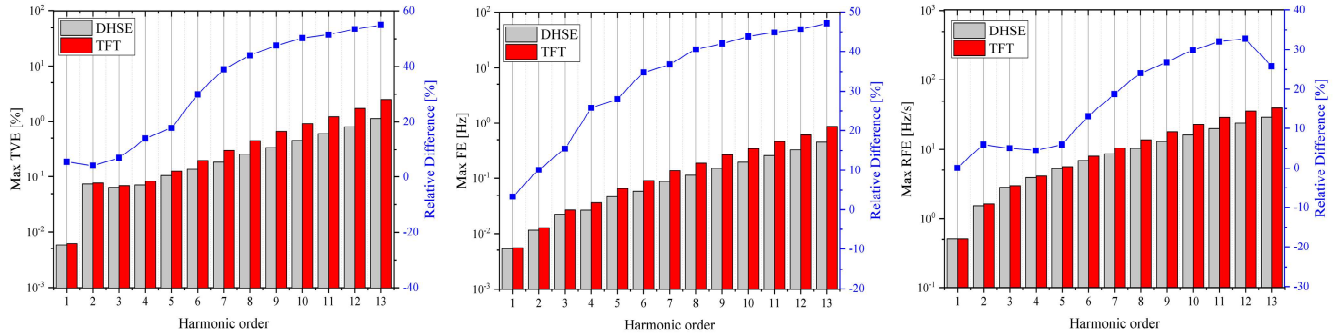


Fig. 13. Results under frequency ramp conditions.

### C. Harmonic Oscillation

As stated in section I, harmonic amplitudes and frequencies (or phases) can be dynamic because of varying loads or sub-synchronous oscillations. The signal in (19) is used for this test, where $k_x$=$k_a$=0.1 are the amplitude and phase modulation factors; and $f_m$=5 Hz is the modulation frequency. These parameters are set according to the M class test of the Standard, which has a stricter test condition than the P class test. Harmonic frequencies are always linear with the fundamental frequency.

$$\begin{aligned} s(t) &= \left(1+k_x\cos 2\pi f_m t\right)\cos\left(2\pi f_0 t + k_a\cos 2\pi f_m t\right) \\ &+0.1\left(1+k_x\cos 2\pi f_m t\right)\cos\left(2\pi h f_0 t + hk_a\cos 2\pi f_m t\right) \\ & h=2,\ldots,13. \end{aligned} \quad (19)$$

In Fig. 12, the corresponding results are shown. As seen, the DHSE is more accurate than the TFT in harmonic synchrophasor, frequency and ROCOF estimation. Further, the higher the harmonic order is, the larger the relative differences between the DHSE's and TFT's PEEs are. Thus, the DHSE performs better than the TFT, especially in high-order harmonics parameter estimation.

The TVE, FE and RFE limits in the Standard for PMUs with reporting rates= 50 frames/s are 3%, 0.3 Hz and 14 Hz/s, respectively. From Fig. 12, we can see that the DHSE can only meet the TVE requirement.

### D. Frequency Ramp

The frequency of a voltage/current signal can have linear changes due to system disturbances. In order to simulate this condition, a test signal shown in (20) is used, where $R_f$=1 Hz/s is the rate of change of the fundamental frequency. Accordingly, the ROCOF of the $h$th harmonic is $hR_f$ [23]. The fundamental frequency is varied from 49.5 to 50.5 Hz linearly.

$$\begin{aligned} s(t) &= \cos\left(2\pi ft+\pi R_f t^2\right)+0.1\cos\left(2\pi hft+\pi hR_f t^2\right) \\ & h=2,\ldots,13. \end{aligned} \quad (20)$$

In Fig. 13, the corresponding results obtained with the DHSE and TFT are given. We can see that the maximum TVEs, FEs and RFEs of the DHSE are smaller than those of the TFT. With the increase in harmonic order, the advantages are more obvious. Again, the DHSE performs better than the TFT, especially in high-order harmonics parameter estimation.

In the standard, the TVE, FE and RFE limits for the M class PMUs are 1%, 0.01 Hz and 0.2 Hz/s, respectively. As for the DHSE, only the 1st~12th harmonic TVEs and fundamental FE can meet the requirements. The maximum FE and RFE of the DHSE are much larger than the thresholds. Similarly, a longer observation window and higher order model can be used to mitigate the impact of the frequency ramps.

### E. Exponentially Decaying Amplitude

Under fault conditions, harmonics can have decaying amplitudes. In order to simulate this condition, a signal shown in (21) is used for the test, where $\beta_h$ is the damping coefficient of the $h$th harmonic. The corresponding parameter values are shown in TABLE II.

$$s(t)=\sum_{h=1}^{13} a_h\left(1+\exp^{-\beta_h t}\right)\cos\left(2\pi hft\right) \quad (21)$$

In TABLE III, the maximum TVEs, FEs and RFEs of the DHSE and TFT are shown. Although the DHSE's estimation accuracy is lower than the TFT's, its maximum TVEs, FEs

TABLE II
THE PARAMETER VALUES IN (22)

| $h$ | 1 | 2 | 3 | 5 | 7 | 9 | 11 | 13 |
|---|---|---|---|---|---|---|---|---|
| $a_h$ | 1 | 0.1 | 0.1 | 0.1 | 0.1 | 0.1 | 0.1 | 0.1 |
| $\beta_h$ | 1.6 | 1.2 | 0.8 | 0.56 | 0.45 | 0.34 | 0.27 | 0.2 |

TABLE III
MAXIMUM TVES, FES, AND RFES OBTAINED WITH THE DHSE AND TFT UNDER EXPONENTIALLY DECAYING AMPLITUDE

| $h$ | TVE [%] | | FE [Hz] | | RFE [Hz/s] | |
|---|---|---|---|---|---|---|
| | DHSE | TFT | DHSE | TFT | DHSE | TFT |
| 1 | 0.00 | 0.00 | 0.00 | 0.00 | 0.01 | 0.00 |
| 2 | 0.00 | 0.00 | 0.00 | 0.00 | 0.08 | 0.01 |
| 3 | 0.00 | 0.00 | 0.00 | 0.00 | 0.09 | 0.01 |
| 5 | 0.00 | 0.00 | 0.00 | 0.00 | 0.11 | 0.00 |
| 7 | 0.01 | 0.00 | 0.00 | 0.00 | 0.14 | 0.00 |
| 9 | 0.02 | 0.00 | 0.00 | 0.00 | 0.17 | 0.00 |
| 11 | 0.03 | 0.00 | 0.00 | 0.00 | 0.23 | 0.00 |
| 13 | 0.06 | 0.00 | 0.00 | 0.00 | 0.08 | 0.00 |

TABLE IV
RESPONSE TIMES OF THE DHSE AND TFT IN AMPLITUDE STEP CHANGE TEST. THE RESULTS ARE EXPRESSED AS NOMINAL CYCLES

| $h$ | TVE | | FE | | RFE | |
|---|---|---|---|---|---|---|
| | DHSE | TFT | DHSE | TFT | DHSE | TFT |
| 1 | 0.92 | 0.91 | 2.97 | 2.97 | 2.98 | 2.98 |
| 2 | 2.92 | 2.92 | 2.96 | 2.96 | 2.99 | 2.99 |
| 3 | 2.92 | 2.91 | 2.99 | 2.99 | 2.98 | 2.98 |
| 4 | 2.91 | 2.91 | 2.99 | 2.99 | 2.99 | 2.99 |
| 5 | 2.91 | 2.91 | 2.99 | 2.99 | 2.99 | 2.99 |
| 6 | 2.90 | 2.90 | 2.99 | 2.99 | 2.99 | 2.99 |
| 7 | 2.12 | 2.12 | 2.99 | 2.99 | 2.99 | 2.99 |
| 8 | 1.30 | 1.30 | 2.99 | 2.99 | 2.99 | 2.99 |
| 9 | 1.26 | 1.26 | 2.99 | 2.99 | 2.99 | 2.99 |
| 10 | 1.23 | 1.23 | 2.99 | 2.99 | 2.99 | 2.99 |
| 11 | 1.21 | 1.20 | 2.99 | 2.99 | 2.99 | 2.99 |
| 12 | 1.20 | 1.19 | 2.99 | 2.99 | 2.99 | 2.99 |
| 13 | 1.66 | 1.59 | 2.99 | 2.99 | 2.99 | 2.99 |

TABLE V
RESPONSE TIMES OF THE DHSE AND TFT IN PHASE STEP CHANGE TEST. THE RESULTS ARE ALSO EXPRESSED AS NOMINAL CYCLES

| $h$ | TVE | FE | RFE |
|---|---|---|---|

| | DHSE | TFT | DHSE | TFT | DHSE | TFT |
|---|---|---|---|---|---|---|
| 1 | 2.43 | 2.43 | 2.89 | 2.89 | 2.83 | 2.83 |
| 2 | 2.84 | 2.84 | 2.92 | 2.91 | 2.97 | 2.97 |
| 3 | 2.84 | 2.84 | 2.96 | 2.96 | 2.96 | 2.96 |
| 4 | 2.84 | 2.84 | 2.97 | 2.97 | 2.97 | 2.97 |
| 5 | 2.83 | 2.83 | 2.97 | 2.97 | 2.97 | 2.97 |
| 6 | 2.72 | 2.71 | 2.97 | 2.97 | 2.97 | 2.97 |
| 7 | 2.64 | 2.63 | 2.99 | 2.99 | 2.97 | 2.97 |
| 8 | 2.66 | 2.66 | 2.99 | 2.99 | 2.99 | 2.97 |
| 9 | 2.59 | 2.59 | 2.99 | 2.99 | 2.99 | 2.99 |
| 10 | 2.53 | 2.53 | 2.99 | 2.99 | 2.99 | 2.99 |
| 11 | 2.47 | 2.40 | 2.99 | 2.99 | 2.99 | 2.99 |
| 12 | 2.37 | 2.28 | 2.99 | 2.99 | 2.99 | 2.99 |
| 13 | 2.54 | 2.54 | 2.99 | 2.99 | 2.99 | 2.99 |

and RFEs for all harmonics estimation are 0.06%, 0.00 Hz and 0.23 Hz/s, respectively. They are very small, and thus can be neglected. In the Standard, there are no TVE, FE and RFE limits for fundamental parameter estimation.

### *F. Step Change*

Under fault conditions, harmonic amplitudes, phases or frequencies may have step changes. For amplitude and phase step change tests, the signal shown in (18) is used. In the first test, the amplitude of each component changes to 110% of the original at the time of $t$=2 s. In the second test, the phases change to $\frac{\pi}{18}$ at $t$=2 s.

In the Standard, the response time is used to evaluate the estimators' performances under step change conditions. It is

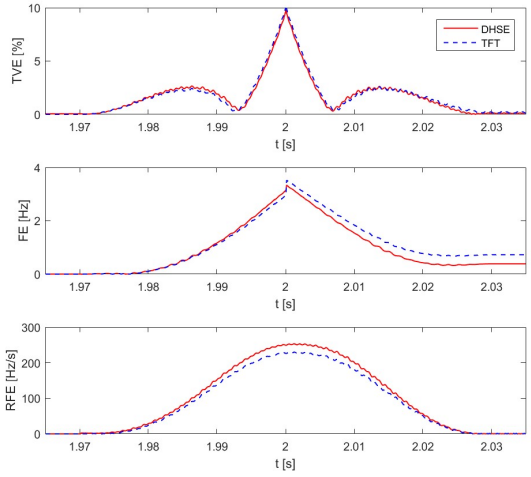


Fig. 14. The TVEs, FEs and RFEs of the 13th harmonic under frequency step change condition.

defined as the time interval between the instant when the PEE (TVE, FE or RFE) is larger than a given threshold at the first and last time. In the Standard, the TVE, FE and RFE thresholds for P class PMUs are 1%, 0.005 Hz and 0.4 Hz/s, respectively. If these requirements are also used for harmonics, the corresponding results are shown in TABLE IV and TABLE V. As seen, in both tests, the response times of the DHSE and TFT are almost the same. For FE and RFE, the response times of the both methods are always about 0.06 ms. However, they are different in different harmonic synchrophasors estimation. This is because the corresponding estimators have different frequency responses.

We also test the estimators' performances under frequency step change conditions. The fundamental frequency of (18) changes to 49.5 Hz at $t$=2 s. Unlike the above two tests, the response times of the DHSE and TFT are not the same anymore. This is because the two methods have different performance under frequency deviation conditions. An example is given in Fig. 15. Generally, the DHSE performs better in response times. Please note that because the maximum FEs and RFEs under steady states are larger than the thresholds, response times cannot be obtained.

### *G. Interharmonic Interferences*

Interharmonics can be significant in power systems. In the Standard, an interfering signal out of the filter passband is considered for synchrophasor measurement. Its frequency varies over a range from below the passband and from above the passband up to the second harmonic. We use a similar scheme for harmonic tests. For example, interharmonics within $[(h\text{-}1)f_0\text{+}0.5(h\text{-}1),\ hf_0\text{-}25]$ and $[hf_0\text{+}25,\ (h\text{+}1)f_0\text{-}0.5(h\text{+}1)]$ Hz are considered for the $h$th harmonic test (reporting rate= 50 frames/s). The test signal is shown in (2).

$$s(t)=\cos(2\pi f_0 t)+0.1\cos(2\pi h f_0 t)+0.05\cos(2\pi f_i t)\quad h=2,\ldots,13 \tag{22}$$

In Fig. 16, the TVEs, FEs and RFEs of the second harmonic are shown. Generally, the ability of interharmonic rejection is determined by the estimator's frequency response (or FIR ripples). For each harmonic estimation, the worst case is when the interharmonic is close to the estimator's passband. By contrast, if the interharmonic is close to other harmonics, the detrimental effect will be very small. In Fig. 17, the maximum TVEs, FEs and RFEs of different harmonics are shown.

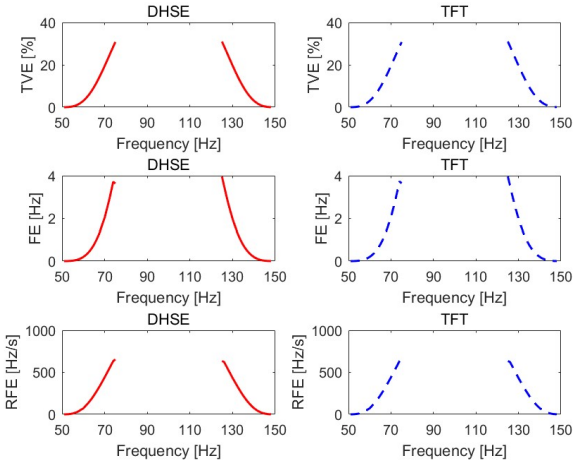


Fig. 16. The TVEs, FEs and RFEs of the second harmonic under different interharmonics interference.

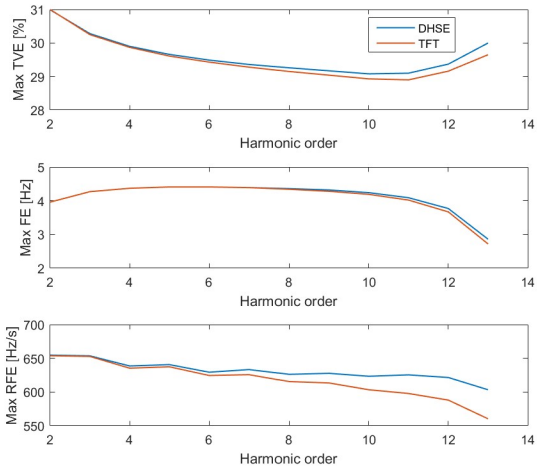


Fig. 17. The maximum TVEs, FEs and RFEs of different harmonics (from the second to the 13th).

For low-order harmonics, the DHSE and TFT have similar performance in harmonic synchrophasor, frequency and ROCOF estimation. However, with the increase of harmonic orders, their differences become bigger.

In the Standard, the corresponding requirements of the TVE and FE of this test condition are 1.3% and 0.01 Hz, respectively. Obviously, the DHSE cannot meet the requirements completely. For example, the maximum TVE, FE and RFE of the second harmonic are 30.99%, 3.96 Hz and 654.68 Hz/s, respectively. Thus, the interharmonic is a main uncertainty contribution in harmonic synchrophasor, frequency and ROCOF estimation. Generally, a long observation window can be used to mitigate the detrimental impact.

### *H. A Practical Example*

In order to demonstrate the DHSE's practical values, a set of current field data is used for the test. In Fig. 18, the field data and its spectrum are shown. As seen, there are significant fundamental and third harmonic components.

The corresponding parameter estimates of the DHSE and TFT are shown in Fig. 19. For better readability, the estimates of the DHSE and TFT are shown separately. We can see that the DHSE's and TFT's amplitude, frequency or ROCOF estimates are almost the same. Thus, for an unknown signal, the DHSE can still be used to estimate harmonic parameters.

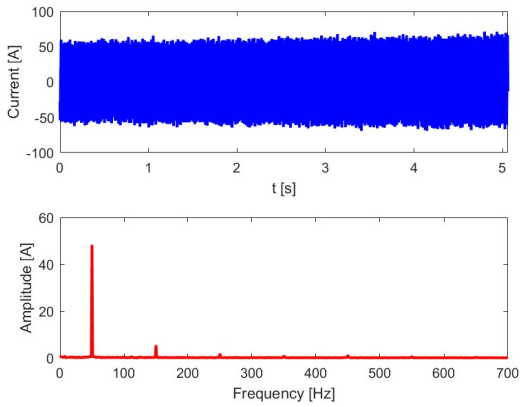


Fig. 18. Current recorded data and its spectrum

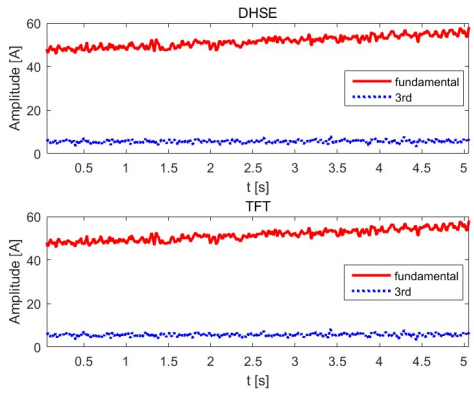


(a)

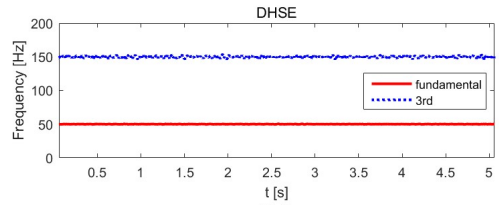


(b)

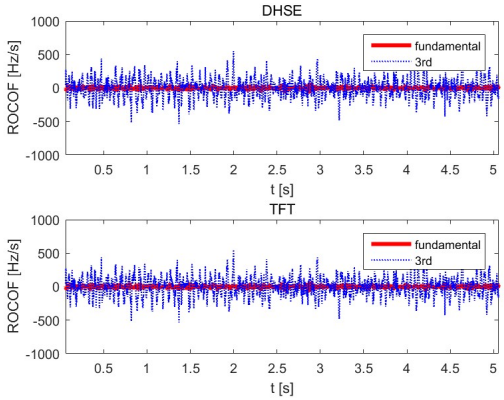


(c)

Fig. 19. Parameter estimates of the DHSE and TFT.

## VII. Conclusion

A novel dynamic harmonic synchrophasor estimator is proposed for dynamic harmonic synchrophasor, frequency and ROCOF estimation. On the basis of the sinc function interpolation, a bank of FIR filters is designed. The parameter $B_h$ is properly selected to obtain good performance in low- and high-order harmonics estimation. The limited computational burden helps it have the possibility of practical implementation. As is shown in the simulation tests, interharmonic interference is a main uncertainty contribution of the DHSE in all parameter estimation. If the Standard for fundamental synchrophasor measurement is also referred for harmonic component measurement, it is shown that the FE and RFE limits are more difficult to meet than the TVE limits. A practical example shows that the DHSE can also be used to process an unknown signal.

Compared with the TFT, the DHSE has lower passband ripples and higher stopband attenuation. Thus, under frequency deviation, harmonic oscillation and frequency ramp conditions, the DHSE is more accurate than the TFT in all parameter estimation.

## Appendix

According to the Shannon sampling theorem, each harmonic synchrophasor $p_h(t)$ can be described as [25]

$$p_h(t)=\sum_{k=-\infty}^{+\infty} p_{k,h}\frac{\sin\left[\pi\left(2Bt-k\right)\right]}{\pi\left(2Bt-k\right)}\quad h=1,\ldots,H \tag{A1}$$

where $p_{k,h}=p_h(k/(2B))$, with $k\in[-\infty,+\infty]$, are the samples of $p_h(t)$ at $t=k/(2B)$ with the sampling rate $2B$. Fig. A1 gives a qualitative representation of the Shannon sampling theorem.

Next, we give an approximate model of (A1) with finite terms.

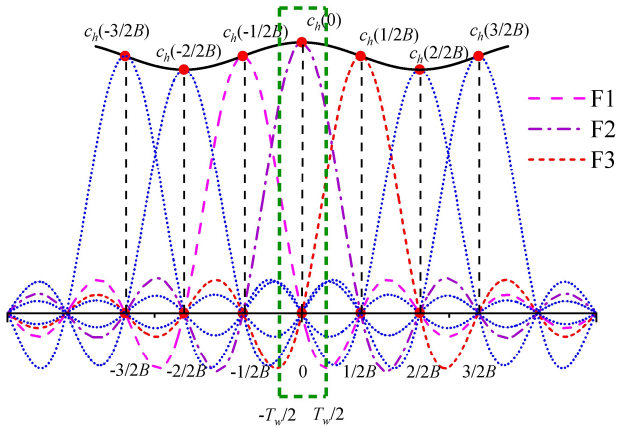


Fig. A1. Qualitative representation of the Shannon sampling theorem

Note that in a limited observation window $[-T_w/2, T_w/2]$, the samples far away from $[-T_w/2, T_w/2]$ have few contributions to the reconstruction of $p_h(t)$. Thus, $p_h(t)$ can be reconstructed by the samples in and around the observation window approximately [26], which is given by

$$p_h^K(t) = \sum_{k=-K}^{+K} p_{k,h} \frac{\sin\left[\pi(2Bt-k)\right]}{\pi(2Bt-k)} \quad -\frac{T_w}{2} \le t \le \frac{T_w}{2} \quad (A2)$$
$$h = 1, \ldots, H$$

where $K$ is the number of samples on both sides of $p_h(0)$. According to the former descriptions, the observation window $T_w$ should meet $T_w<K/B$.

## REFERENCES


[1] I. Kamwa, R. Grondin, and D. Mcnabb, "On-line tracking of changing harmonics in stressed power systems: application to Hydro-Quebec network," *IEEE Transactions on Power Delivery*, vol. 11, no. 4, pp. 2020-2027, 1996.

[2] D. Miodrag Kušljević, J. Josif Tomić and D. Poljak, Predrag, "Maximally Flat-Frequency-Response Multiple-Resonator-Based Harmonic Analysis," *IEEE Transactions on Instrumentation & Measurement*, vol. PP, no. 99, pp. 1-12, 2017.

[3] L. Asiminoaei, F. Blaabjerg, and S. Hansen, "Detection is key - Harmonic detection methods for active power filter applications," *IEEE Industry Applications Magazine*, vol. 13, no. 4, pp. 22-33, 2007.

[4] I. Kamwa, L. Geoffroy, S. R. Samantaray, and A. Jain, "Synchrophasors data analytics framework for power grid control and dynamic stability monitoring", *IET Engineering & Technology Reference*, pp. 1-22, 2016. DOI: 10.1049/etr.2015.0049.

[5] M. A. Platas-Garza and J. A. de la O Serna, "Dynamic harmonic analysis through Taylor–Fourier transform," *IEEE Transactions on Instrumentation & Measurement,* vol. 60, pp. 804-813, 2011.

[6] A. Carta, N. Locci, and C. Muscas, "GPS-based system for the measurement of synchronized harmonic phasors," *IEEE Transactions on Instrumentation & Measurement*, vol. 58, no. 3, pp. 586-593, 2009.

[7] A. Carta, N. Locci, and C. Muscas, "A PMU for the measurement of synchronized harmonic phasors in three-phase distribution networks," *IEEE Transactions on Instrumentation & Measurement,* vol. 58, no. 10, pp. 3723-3730, 2009.

[8] "*IEEE Standard for Synchrophasor Measurements for Power Systems*," IEEE Std C37.118.1-2011 (Revision of IEEE Std C37.118-2005), 2011.

[9] "*IEEE Standard for Synchrophasor Measurements for Power Systems—Amendment 1: Modification of Selected Performance Requirements,*" IEEE Standard C37.118.1a-2014 (Amendment to IEEE Standard C37.118.1-2011), Apr. 2014.

[10] M. Chakir, I. Kamwa, and H. L. Huy, "Extended C37.118.1 PMU algorithms for joint tracking of fundamental and harmonic phasors in stressed power systems and microgrids," *IEEE Transactions on Power Delivery,* vol. 29, no. 3, pp. 1465-1480, 2014.

[11] "*General guide on harmonics and interharmonics measurements for power supply systems and equipment connected thereto*," IEC 61000-4-7, 2002.

[12] J. A. de la O. Serna and J. Rodríguez-Maldonado, "Taylor–Kalman–Fourier Filters for Instantaneous Oscillating Phasor and Harmonic Estimates," *IEEE Transactions on Instrumentation & Measurement,* vol. 61, pp. 941-951, 2012.

[13] R. Ferrero, P. A. Pegoraro, and S. Toscani, "Dynamic fundamental and harmonic synchrophasor estimation by Extended Kalman filter," *IEEE International Workshop on Applied Measurements for Power Systems*, pp. 1-6, 2016.

[14] J. Liu, F. Ni, P. A. Pegoraro, F. Ponci, A. Monti, and C. Muscas, "Fundamental and harmonic synchrophasors estimation using modified Taylor-Kalman filter," *IEEE International Workshop on Applied Measurements for Power Systems*, pp. 1-6, 2012.

[15] L. Fu, J. Zhang, S. Xiong, Z. He, and R. Mai, "A modified dynamic synchrophasor estimation algorithm considering frequency deviation," *IEEE Transactions on Smart Grid*, vol. 8, no. 2, pp. 640-650, 2017.

[16] J. A. De La O Serna, "Synchrophasor Measurement With Polynomial Phase-Locked-Loop Taylor–Fourier Filters," *IEEE Transactions on Instrumentation & Measurement*, vol. 64, no. 2,pp. 328-337, 2015.

[17] P. Castello, T. Liu, C. Muscas, P. A. Pegoraro, F. Ponci, and A. Monti, "A Fast and Accurate PMU Algorithm for P+M Class Measurement of Synchrophasor and Frequency," *IEEE Transactions on Instrumentation & Measurement*, vol. 63, no. 12, pp. 2837-2845, 2014.

[18] M. A. Platas-Garza, and J. A. de la O Serna, "Polynomial Implementation of the Taylor–Fourier Transform for Harmonic Analysis," *IEEE Transactions on Instrumentation & Measurement*, vol. 63, no. 12, pp. 2846-2854, 2014.

[19] M. Bertocco, G. Frigo, C. Narduzzi, C. Muscas, and P. A. Pegoraro, "Compressive Sensing of a Taylor-Fourier Multifrequency Model for Synchrophasor Estimation," *IEEE Transactions on Instrumentation & Measurement*, vol. 64, no. 12, pp. 3274-3283, 2015.

[20] G. Frigo, G. Giorgi, M. Bertocco, and C. Narduzzi, "Multifunction phasor analysis for distribution networks," *IEEE International Workshop on Applied Measurements for Power System*, pp. 1-6, 2016.

[21] G. Frigo, G. Giorgi, and C. Narduzzi, "Efficient detection for multifrequency dynamic phasor analysis," *IEEE International Workshop on Applied Measurements for Power Systems*, pp. 1-6, 2016.

[22] C. Narduzzi, M. Bertocco, G. Frigo and G. Giorgi, "*Fast-TFM--Multifrequency Phasor Measurement for Distribution Networks*," in IEEE Transactions on Instrumentation and Measurement, vol. PP, no. 99, pp. 1-11. doi: 10.1109/TIM.2018.2809080

[23] S. K. Jain, P. Jain, and S. N. Singh, "A fast harmonic phasor measurement method for smart grid applications," *IEEE Transactions on Smart Grid,* vol. 8, pp. 493-502, 2016.

[24] J. A. de la O Serna, "Dynamic Phasor Estimates for Power System Oscillations," *IEEE Transactions on Instrumentation & Measurement*, vol. 56, no. 5, pp. 1648-1657, 2007.

[25] C. E. Shannon, "A mathematical theory of communication," *The Bell System Technical Journal,* vol. 27, pp. 623-656, 1948.

[26] F. Wang, X. Jin, Z. Wang. "Optimal Design of FIR Digital Filters for Dynamic Phasor Measurement," *Proceedings of the CSEE*, vol. 34(15), pp. 2388-2395, 2014.

[27] F. Wang, W. Zhao, L. Guo, C. Wang, X. Jiang, and Z. Wang, "Optimal filter design for frequency and synchrophasor measurement," *Proceedings of the CSEE,* vol. 37(22), pp. 6691-6699+6782, 2017.

[28] *"Power quality-Frequency deviation for power system,"* GB/T 15945-2008, 2008.

[29] "*Test specification for synchrophasor measurement unit for power systems*," GB/T 26862-2011.


**Lei Chen** received his B.S. degree from North China Electric Power University in China in 2015. He is currently a Ph.D. student in Tsinghua University. His research interests include digital power metering systems, power quality monitoring, and harmonic analysis in power systems.

**Wei Zhao** received his Ph.D. degree from Moscow Energy Institute, Russia, in 1991. Currently, he is a professor with the Department of Electrical Engineering, Tsinghua University. His research areas include electromagnetic measurement, virtual instrumentation, networked instrumentation system, cloud based instrumentation.

**Qing Wang** received her Ph.D. degree from De Montfort University, UK in 2001. Currently, she is an Associate Professor with the Department of Engineering at Durham University. Her research interests include electronic instruments and measurement, computer simulation and advanced manufacturing technology. Dr. Wang is a Charted Engineer (CEng), a senior member of IEEE (SMIEEE), a member of IMechE (MIMechE), a member of ASME (MASME) and a Fellow of the Higher Education Academy (FHEA).

**Fuping Wang** received his Ph.D. degree from Tsinghua University in 2002. Currently, he is an associate research fellow with the Department of Electrical Engineering at Tsinghua University. His current research interests are circuits and systems and signal processing.

**Songling Huang** received his Ph.D. degree from Tsinghua University in 2001. Currently, he is a professor with the Department of Electrical Engineering, Tsinghua University. His current research interests are electromagnetic measurement and nondestructive evaluation.